Deep Learning-Enabled Non-Invasive Human ECG and Long-Term Heart Rate Variability Monitoring and Matching with Sleep Stages Based on an Optical Fiber Sensor System

Haochun Gao, Qing Wang, *Member*, *IEEE*, Ke Li, *Student Member*, *IEEE*, Jing Zhou, *Student Member*, *IEEE*, Xiang Wang, Changyuan Yu, *Senior Member*, *IEEE*, *Fellow*, *OSA*

***Abstract*—Optical fiber sensors, known for their small size, lightweight, and resistance to electronic interference, are widely used in various applications, including medical vital signs monitoring and Internet of Medical Things (IoMT). They are particularly useful in recording electrocardiogram (ECG) signals and measuring heart rate variability (HRV), which provides insights into the autonomic nervous system activity. HRV, affected by sleep quality, can be used to assess sleep stages. Monitoring ECG and HRV during sleep can identify sleep disruptions and guide interventions to improve sleep quality. However, existing optical fiber sensors for vital signs monitoring have some drawbacks, including signal loss, sensitivity to light source intensity changes, signal distortion during long-distance transmission, and high manufacturing and maintenance costs. They also may produce missing or anomalous data due to sensor failures, transmission and storage issues, or other unforeseen factors. Conventional monitoring methods can be uncomfortable for long-term daily ECG and HRV monitoring. To address these problems, we propose a novel optical fiber sensor based on fiber interferometer and a robust semi-supervised framework, termed EBLA, which is composed of CEDANN and GSCM modules, can reconstruct and analyze raw ECG signals, extract temporal and spatial features, and match the relationship between HRV and sleep stages. The framework also applies external knowledge of acquired signal for graph modeling for the first time, revealing data relationships and better understanding the global sample structure from the raw ECG signal. The average root mean square error (RMSE) and mean absolute error (MAE) of experiments reach 1.711 and 1.196, respectively, demonstrating its feasibility and effectiveness, exhibiting a better effect and its superior to the state-of-the-art approaches. This work has the potential to promote the smart healthcare monitoring and application of optical fiber sensing.**

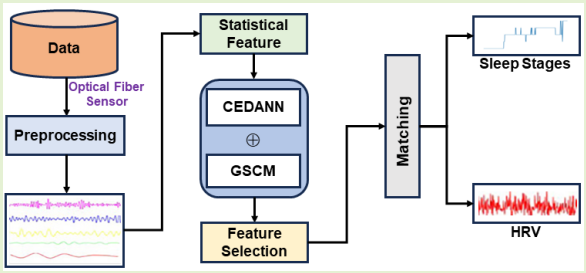

***Index Terms*—Electrocardiogram (ECG), Heart Rate Variability (HRV), Sleep Stage, Vital Signs, Optical Fiber Interferometer, Deep Learning, Healthcare Monitoring**

I. INTRODUCTION

Over the past few years, the optical fiber communication industry has been leaping forward. And the optical fiber communication system has been reported with several characteristics, such as larger channel bandwidth, lower cost, and more reliable information service [1]-[4]. Moreover, optical fiber sensors have been extensively employed for a wide variety of applications, especially in medical monitoring [5]-[8]. Currently, the incidence and mortality of a wide variety of high-risk diseases tend to be increased. With the progress in modern medicine and the shift of priority from the treatment to health detection in terms of humans, daily evaluation on the day-to-day basis, and prevention turn out to take on critical significance in preventing and controlling the development of high-risk diseases [9]. For

(Corresponding author: Qing Wang, Changyuan Yu)
H. Gao, Q. Wang and J. Zhou are with the Department of Electrical and Electronic Engineering, The Hong Kong Polytechnic University, Hong Kong (e-mail: haochun.gao@connect.polyu.hk, qing-wq.wang@connect.polyu.hk, jinge.zhou@connect.polyu.hk).
K. Li is with the School of Fashion and Textile, The Hong Kong Polytechnic University, Hong Kong (e-mail: ke0414.li@connect.polyu.hk).
X. Wang is with the Department of Engineering, University of Cambridge, United Kingdom (e-mail: xw438@cam.ac.uk).
C. Yu is with the Department of Electrical and Electronic Engineering, The Hong Kong Polytechnic University, Hong Kong, and also with the Shenzhen Research Institute, The Hong Kong Polytechnic University, Shenzhen 518057, China (e-mail: changyuan.yu@polyu.edu.hk).

example, the vital signs of patients are an important piece of data needed for the treatment and care of patients, especially when the continuous monitoring of heart rate is required. A wide variety of vital signs, such as blood oxygen, pulse, blood pressure (BP), heartbeat, respiration, and body temperature, have been confirmed as major health indicators of human physiological activities. Accordingly, vital signs monitoring can facilitate daily health condition evaluation of subjects and supporting the early diagnosis of certain diseases, such as cardiovascular and cerebrovascular diseases [10], [11]. To be specific, heartbeat and respiratory signals are the most common ones, which are closely related to health status [12]-[15]. However, the method common to monitor vital signs, namely five-lead detection, requires the direct contact with human skin to collect vital signs signal. In different scenarios, the above-mentioned measurement results in inconvenience, and it performs poorly in efficiency and accuracy, thus causing disruption to timely and effective treatment. The above-described issue can be effectively addressed by using optical fiber sensors [16], [17].

Electrocardiogram (ECG) signal is one of the most important vital signs that is used to record the electrical activity of the heart, providing information about the function and condition of heart. In addition, during medical emergencies, monitoring ECG signals can guide emergency treatment such as cardiopulmonary resuscitation [18]. Overall, ECG signal plays an important role in vital signs monitoring, can provide timely and accurate physiological information, and play a key role in the early detection, diagnosis and treatment of diseases. Heart rate variability (HRV) has been reported as a physiological measure that quantifies the change of successive heartbeat time intervals [19]. It is considered a reliable indicator of autonomic nervous system activity. HRV is usually derived from an ECG signal [20]. By analyzing the ECG signal, one can determine the intervals between heartbeats and thus calculate the HRV. The ECG provides the raw data, while the HRV provides a meaningful interpretation of that data in terms of heart health. High HRV is generally a sign of a healthy heart, as it indicates that the heart is able to adapt to different situations and conditions. Conversely, low HRV is often a sign of stress or illness. The integration of HRV monitoring with sleep condition detection and the Internet of Medical Things (IoMT) has achieved significant attention [21]. Sleep condition detection involves monitoring and analyzing a wide variety of parameters during sleep for the evaluation of sleep patterns and quality. HRV is a valuable biomarker in terms of sleep-associated conditions and disorders, such as insomnia, sleep apnea, and sleep disturbances. By measuring HRV during sleep, it is possible to identify abnormalities or deviations from normal patterns, which can facilitate sleep disorder diagnosis and management. The IoMT is the network of interconnected devices that collect, exchange, and analyze data to enable communication and automation in a wide variety of domains [22], [23]. In the context of sleep condition detection, IoMT devices, such as wearable fitness trackers, smartwatches, and sleep monitoring systems can be employed to capture HRV data during sleep. The above-mentioned devices can continuously monitor HRV and transmit the data to a central server or cloud-based platform for analysis [24]. By integrating HRV monitoring with IoMT technologies, several benefits can be realized. Firstly, the continuous monitoring of HRV during sleep provides a more comprehensive and accurate assessment of sleep quality compared to conventional subjective methods. This data can be further analyzed using machine learning algorithms to detect patterns, trends, and anomalies indicative of sleep disorders. Second, IoMT devices can provide real-time feedback and interventions based on HRV measurements. For example, if the HRV indicates high levels of stress or arousal during sleep, IoMT devices can trigger interventions such as adjusting the room temperature, playing soothing sounds, or providing relaxation techniques to promote better sleep [25]-[27]. Furthermore, the integration of HRV monitoring with IoMT contributes to remote monitoring and telemedicine applications. Healthcare professionals can access HRV data remotely while providing personalized recommendations or interventions to subjects with sleep stages, improving the accessibility and convenience of healthcare services. In brief, the integration of HRV monitoring, sleep condition detection, and the IoMT holds great potential for advancing the field of sleep medicine [28], [29].

Recently, some optical fiber sensors based on banding loss have been developed to monitor human vital signs, such as ballistocardiography (BCG) and ECG signal, with the aim of extracting and detecting human heart rate (HR), respiratory rate (RR), HRV, and so on [30], [31]. Although this optical fiber sensor is efficient, there are some drawbacks. Banding loss might imply a loss of signal quality or degradation within specific frequency bands, leading to reduced performance in certain applications. In this sensor, optical fibers are delicate and can be easily damaged, affecting the performance of the sensor. This can be a concern in harsh environments or industrial settings. Optical fiber sensors are sensitive to temperature changes, which can lead to inaccuracies in measurements. And the optical fiber sensor may be susceptible to external sources of noise and electromagnetic interference, impacting the reliability of measurements. Despite the progress in optical fiber technology, there remains a threshold for the permissible bending of a fiber before the signal loss reaches an unacceptable level. This limitation can be a significant drawback in applications where fibers need to be routed through tight spaces or around sharp corners [32]. In addition, due to the failure of optical fiber sensor in some cases, improper transmission and storage, or other reasons, data missing and data anomaly may result from the use of optical fiber sensor to monitor vital signs signal, such as ECG signal. The quality of the ECG signal will directly affect the accuracy of the extracted HRV. Moreover, with the development of artificial intelligence, while HRV processing with some developed machine learning methods has shown promise in a wide variety of applications, HRV analysis heavily relies on accurate and reliable raw data [33]. And the developed machine learning methods require high-quality data for effective training and inference, which might not encompass the full range of HRV patterns and variations present in the broader population.

To tackle down the above-described issues, a novel optical fiber sensor is proposed based on fiber interferometer, which

utilizes the interference of light waves within an optical fiber to measure a wide variety of physical quantities. The proposed optical fiber sensor is likely to exhibit great sensitivity, such that precise and accurate measurements can be carried out. In addition, EBLA, a new deep learning model is proposed, which can be applied to process the HRV data during human sleep and detect human sleep stages better combined with the proposed optical fiber sensor. Furthermore, the proposed EBLA model can be adopted to long-term human HRV processing for more effective future human sleep condition monitoring and assessment.

The main contributions of this paper are summarized as follows:

(1) A novel interferometer fiber-based optical fiber sensor is newly proposed to monitor human vital signs effectively, such as BCG, ECG and HRV, and shows its superiority over other sensors;

(2) To extract the spatial and temporal features of the acquired vital signs signal for mapping relationship between HRV and sleep conditions, a novel deep learning framework, termed EBLA, is proposed. The external knowledge of acquired data is applied for graph modeling for the first time to reveal the data relationship and obtain the global sample structure better;

(3) An ECG dataset and an HRV dataset following the proposed optical fiber sensor are built for the first time, which is collected from over 300 subjects during sleep;

(4) In combination with the EBLA framework, the proposed optical fiber sensor system can be extensively applicable in non-invasive sleep monitoring, smart health care, and optical fiber sensing applications.

We present the following structure of this paper below. Section II discusses about some methods and the structure of the proposed framework. In Section III, various experiments and the ablation studies compared with other variant models are conducted. In Section IV, the results achieved through experiments are analyzed and discussed. In Section V, the conclusion is drawn and future works are outlined.

II. Materials And Methods

A. Proposed Optical Fiber Sensor

In previous study, we proposed a microbend optical fiber sensor system to monitor perioperative infants' vital signs signal, which is based on banding loss. The microbend optical fiber sensor comprises a segment of graded multimode optical fiber firmly secured between a set of microbenders. Its operational principle is rooted in the concept of optical fiber microbending. As the distance varies between the two microbenders, the sinusoidal amplitude of the clamped multimode optical fiber fluctuates in response to the subtle vibrations generated by an infant's respiration, heartbeats, and other movements. This alteration in the spacing between microbenders results in a modulation of light intensity within the microbend fiber, effectively capturing and reflecting the body's vibrations or motions. Fig. 1 shows the basic mechanism of the microbend optical fiber sensor system.

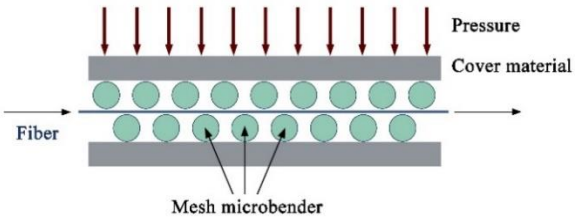

Fig. 1. Basic mechanism of microbend optical fiber sensor system.

In this study, a 1550nm distributed-feedback (DFB) laser is used as the light source in the optical fiber sensor system. Since the optical fiber sensor is based on the principle of interference, the changes of the external environment may cause the random phase drift of the sensor, which will make the working point of the fiber optic interferometer deviate from the center of the linear region. The random drift of the working point can seriously affect the working state of the interferometer. Thus, a 3×3 demodulation method was applied for analyzing the BCG and ECG signal, that is to say, using a 3×3 coupler to divide the interference light into three beams with a phase difference of 120°. The light emitted from the DFB laser is transmitted into the reference and sensing fibers through a 1×2 coupler. Then the beams of light transmitting in the reference and sensing arms will interfere at the 3×3 coupler. The output light intensity of the interferometer can be calculated by using the equation below:

$$I_k = D + I_0 \cos[\varphi(t) - (k-1)(2\pi/3)] \quad (1)$$

where $\varphi(t)$ is the phase difference of light signals, D is the average value of output light intensity, I_0 is the peak intensity of interference fringes, k is the number of the output light path, and k=1, 2, 3.

In practical application, $\varphi(t)$ includes phase changes caused by the measured information and the environment variation which can be denoted as

$$\varphi(t) = \phi(t) + \psi(t) \quad (2)$$

where $\varphi(t)$ represents the signal to be measured, and $\psi(t)$ is the phase difference caused by environmental changes.

The signal light emitted from a broadband source (BBS, SLED-1488/1650-10-FA-B, Shanghai Mai Xuan Laser CO., LTD) is launched into the interferometric optical fiber sensor and the transmission spectrum is detected by an optical spectrum analyzer (YOKOGAWA AQ6370D) with a resolution of 0.01nm, which is shown in Fig. 2. Four interference dips can be observed in the spectrum at wavelengths 1549.4nm, 1549.72nm, 1550.03nm, and 1550.34nm, respectively. All these dips can be used for ECG sensing.

Fig. 2 (b) shows an example of optical fiber consisting of single-mode fiber (SMF) and thin-core fiber (TCF). The working principle of SMF is based on total internal reflection of light. The core is very thin, usually around 8-10μm in diameter. When the light signal enters the core, due to the refractive index difference between the core and the cladding, as long as the light is incident at a certain angle, total internal reflection will occur at the interface between the core and the cladding, so that the light

signal is confined to propagate in the core. This single-mode transmission method can effectively reduce the dispersion of the signal, allowing the light signal to maintain a low attenuation during long-distance transmission, thereby achieving high-speed and long-distance data transmission. TCF also relies on total internal reflection. The core is thinner than that of single-mode fiber, generally 3-5μm. This thinner core can enhance the interaction between light and matter. Due to the core is thin, the distribution of the light field in it is more concentrated, it is more sensitive to slight changes in the external environment, such as changes in temperature, pressure, and refractive index. In sensing applications, it can more accurately detect changes in light signals caused by these changes.

According to the equation (1), the three optical intensity signals can be demodulated by the 3×3 coupler demodulation scheme shown in Fig. 3. The 3×3 coupler is composed of two SMFs and one TCF. The two SMFs are mainly used to input and output optical signals, and the TCF plays a key role in interference. The three optical fibers are fused together in a certain way. In the fusion area, the cores of the optical fibers are close to each other, so that light can be coupled between them. After the light is input from an SMF, it will be coupled into the TCF in the fusion area. Due to the special properties of the TCF, when the light propagates in it, a special light field distribution will be generated due to the thin core. When the light propagates in the TCF, it will interfere with the light coupled in from another SMF.

When light enters the 3×3 coupler, interference occurs inside the coupler. Since the 3×3 coupler has three input ports and three output ports, the light is divided into three paths, and there is a phase difference between these light paths. The intensity of the three output lights will change with the phase change of the input light. When the measured quantity changes, the optical path in the optical fiber sensor will change, causing the phase of the light to change. This phase change will be reflected as a change in light intensity at the output end of the 3×3 coupler. By detecting the light intensity changes at the three output ports, the light intensity changes are converted into phase change information through differentiation and linear algebra operations. The phase change information is corresponded to the physical quantities being measured, such as temperature and pressure changes, so that the size and change of the physical quantity detected by the optical fiber sensor can be demodulated according to the changes in the output light intensity of the 3×3 coupler.

After the differentiation and cross-multiplication operation, the demodulated signal is

$$N = a(e-f) + b(f-d) + c(d-e) = \frac{3\sqrt{3}}{2} I_0^2 \varphi'(t) \quad (3)$$

In the actual environment, fluctuations of the light intensity and changes of the polarization state will influence the value of I_0. To eliminate the influence factors, the following mathematical treatment is carried out.

(a) The data acquisition (DAQ) card

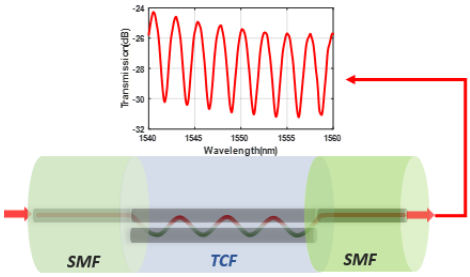

(b) SMF and TCF in the optical fiber

Fig. 2. Vital signs monitoring system based on optical fiber sensor.

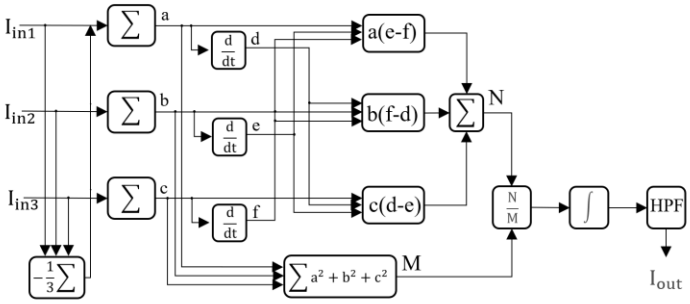

Fig. 3. Demodulation principle of the 3×3 coupler.

First, square the three input signals to obtain

$$M = a^2 + b^2 + c^2 = \frac{3I_0^2}{2} \quad (4)$$

Then divide N by M and eliminate I_0^2 to get

$$P = \frac{N}{M} = \sqrt{3}\varphi'(t) \quad (5)$$

After integral operation, the output is described as

$$\sqrt{3}\varphi(t) = \sqrt{3}\phi(t) + \psi(t) \quad (6)$$

$\psi(t)$ is regarded as a slow change quantity, which can be filtered out through a high-pass filter. I_{out} is the output signal of the 3×3 demodulation scheme, which is known as the ECG signal transmitted to the computer. Basic structure of the proposed system is shown in Fig. 4.

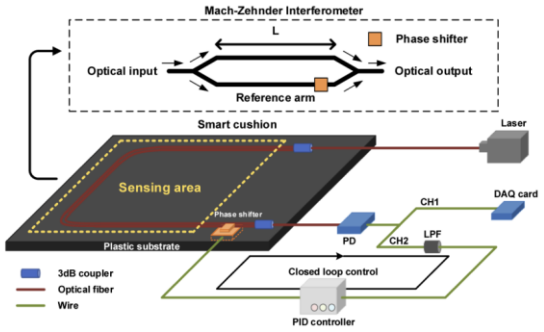

Fig. 4. Structure of the proposed vital signs signal monitoring system.

We have made a better grounding design to make the system more stable and improve the stability of the system, which can reduce the impact of interference signals. Meanwhile, during the experiment, the subjects were kept as calm as possible to minimize the adverse effects of their body movements on the results. Overall, compared with banding loss-based optical fiber sensors, the proposed optical fiber interference-based optical fiber sensor has the characteristics of light weight, compact structure, flexible geometry, explosion-proof, and anti-electromagnetic interference. It has higher sensitivity in vital signs monitoring. Fig. 5 shows the proposed optical fiber sensor system embedded in smart mat.

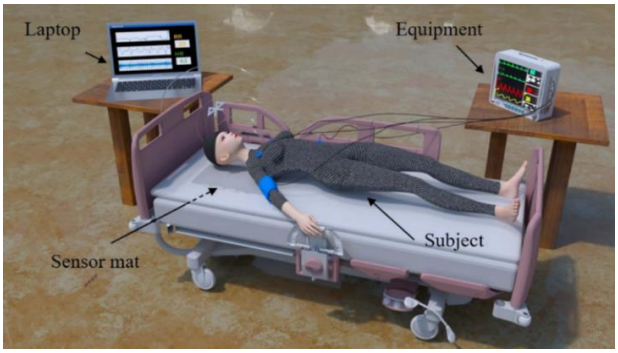

Fig. 5. The proposed optical fiber sensor system embedded in smart mat.

B. Data Acquisition and Processing

HRV is the variation in the time intervals between consecutive heartbeats, also known as inter-beat intervals (IBIs) or R-R intervals. It is a measure of the beat-to-beat changes in heart rate and is affected by the autonomic nervous system, which regulates the balance between sympathetic (fight-or-flight) and parasympathetic (rest-and-digest) activities.

HRV is considered as an important indicator of the functioning of the autonomic nervous system and has been linked to a wide variety of physiological and psychological factors. Higher HRV generally indicates better cardiovascular health and greater adaptability to stress, while lower HRV shows a relationship to elevated risk of cardiovascular disease, poor health outcomes, and reduced resilience to stress.

The major steps for extracting HRV are elucidated in the following:

(1) Data acquisition: The first step is to collect ECG data, which measures the electrical activity of the heart. This is usually done using specialized ECG devices or wearable heart rate monitors that are capable of recording the R-R intervals accurately. Fig. 6 illustrates the ideal ECG signal.

(2) Preprocessing: The recorded ECG data may cover noise and artifacts that need to be removed to ensure accurate HRV analysis. Preprocessing techniques such as filtering, artifact removal, and signal normalization are applied to enhance the quality of the data.

(3) R-peak detection: The R-peaks in the ECG signal corresponded to the highest points of the respective heartbeat. Detecting the above-mentioned R-peaks accurately is crucial for extracting the IBIs. A wide variety of algorithms, such as peak detection algorithms or template matching, are employed to locate the R-peaks. Fig. 7 shows the graph of R-R intervals during time.

(4) Inter-beat interval calculation: Once the R-peaks are detected, the IBIs are calculated by measuring the time intervals between consecutive R-peaks. The above-described IBIs represent the instantaneous heart rate variability. Fig. 8 shows the histogram of R-R intervals.

(5) HRV analysis: HRV can be analyzed in time and frequency domains, such that different insights can be gained into the autonomic nervous system. Some common HRV analysis methods are presented as follows: (a) Time Domain Analysis: This involves analyzing statistical measures derived from the IBIs, such as root mean square of successive differences (RMSSD), standard deviation of the IBIs (SDNN), and the mean R-R interval; (b) Frequency Domain Analysis: The IBIs are transformed into the frequency domain using techniques like the Fourier transform or autoregressive modeling. Next, the power spectrum is investigated for assessing the distribution of power across different frequency bands. The main frequency bands of interest are very low frequency (VLF): <0.04Hz; low frequency (LF): 0.04~0.15Hz and high frequency (HF): 0.15~0.4Hz. The LF component shows a relationship to both sympathetic and parasympathetic activity, while the HF component is primarily affected by parasympathetic activity.

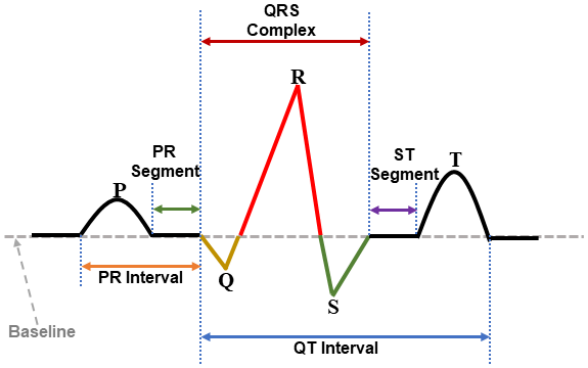

Fig. 6. Ideal ECG signal.

(6) Interpretation: The obtained HRV measures can be

interpreted for clarifying autonomic function, stress levels, and overall cardiovascular health. For example, a higher SDNN and RMSSD in time domain analysis, and higher power in the HF band of the frequency domain analysis, generally indicate better cardiovascular health.

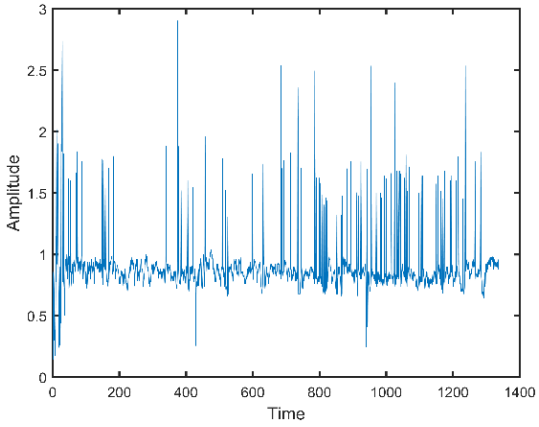

Fig. 7. Graph of R-R intervals against time.

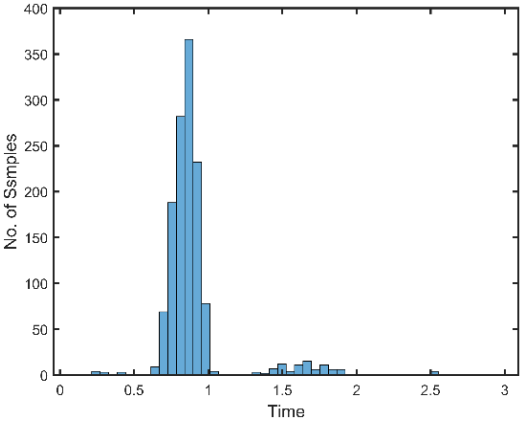

Fig. 8. Histogram of R-R intervals.

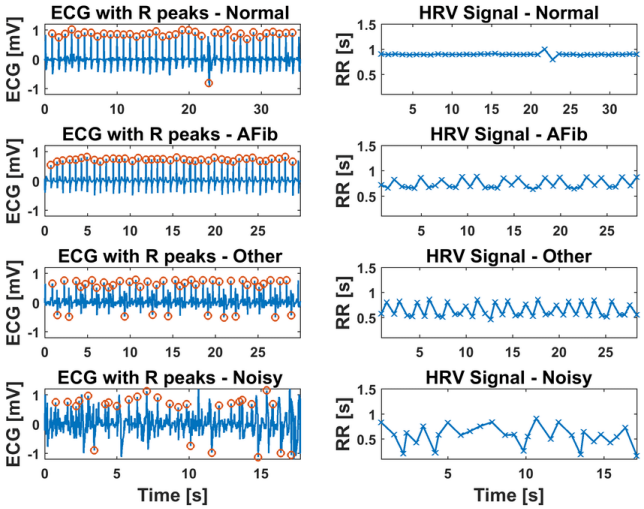

Fig. 9. HRV extracted from the raw ECG signal.

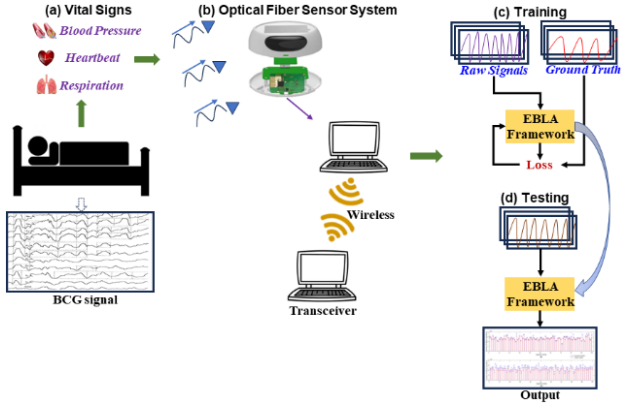

Fig. 10. Whole architecture of the proposed monitoring system.

It is worth noting that HRV analysis can be complex, and various mathematical and statistical techniques are employed for accurate extraction and interpretation. Software tools and dedicated HRV analysis packages are available to simplify the process and provide comprehensive HRV insights. Fig. 9 shows the basic mechanism of extracting HRV from the raw ECG signal with the proposed optical fiber sensor.

Fig. 10 shows the whole process of the proposed monitoring system. It should be noted that the second part is not just another part of the framework. It plays a more significant role as it serves as the final target classifier. This means that the results from this part are the ones that are ultimately used for the final classification of the target data. This highlights the importance of the second part in the overall framework, as it directly influences the final output.

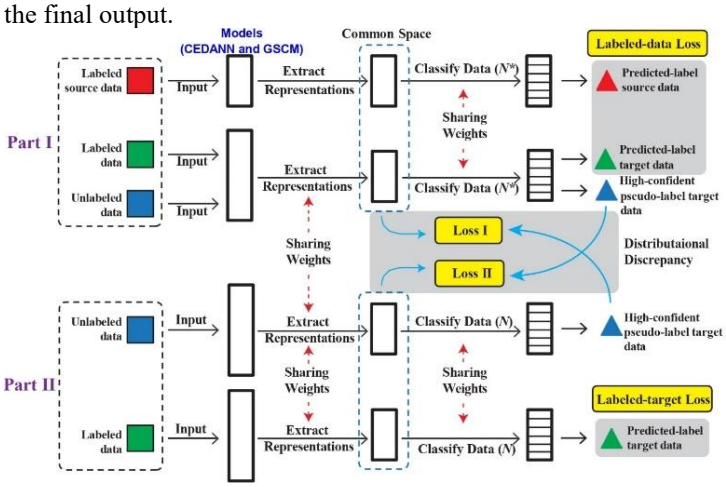

Fig. 11. Overall architecture of EBLA framework in the experiment setup.

As shown in Fig. 11, the first part of the EBLA framework is designed to handle three types of data inputs: labeled source data, labeled target data, and unlabeled target data. The primary objective of this part is to train a classifier that can effectively distinguish between source and target representations. This involves a complex process of analyzing the data, identifying patterns, and creating a model that can accurately classify the data based on these patterns. On the other hand, the second part operates differently. It only deals with two types of data inputs: labeled and unlabeled target data. The main goal is to train a

classifier that is specifically tailored to handle target representation. This involves a more focused approach, as it only deals with target data.

In summary, as shown in Fig. 12, for the data and signal processing part, we use the proposed sensor based on optical fiber interferometer to collect raw ECG data. Then we pre-process the data to remove noise and pseudo-shadow. We calculate IBIs and R-R intervals through detection of R-peaks, analyze HRV data, including time and frequency domain analysis. After that, the HRV data is made of abnormal value correction, lack of value filling and processing. We apply the proposed CEDANN module to decompose mode of data, then process it by bi-directional LSTM (BiLSTM) model, and optimize the weight with attention mechanism. Finally, through the proposed GSCM module, sleep stage classification is achieved based on graph modeling and label propagation.

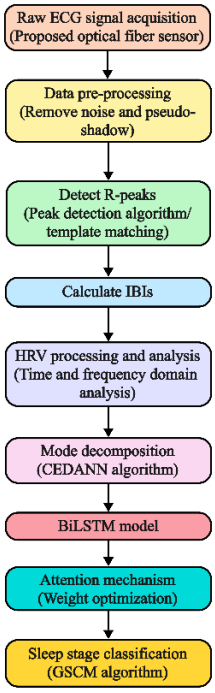

Fig. 12. Flowchart of data and signal processing.

C. Proposed Mode Decomposition Model (CEDANN)

Following the empirical mode decomposition (EMD) [34] and ensemble empirical mode decomposition (EEMD) [35] algorithms, the complete ensemble empirical mode decomposition method for HRV processing during sleep, termed CEDANN, is proposed by us. Although the algorithm of EEMD is capable of alleviating the mode aliasing issue through the addition of Gaussian white noise, some amplitude noise signals exist in the decomposition component. The increase of the number of ensemble averages will lead to the reduced content of noise, whereas mean envelope screening times can be increased, and program running time turns out to be excessively long, which lacks advantages in real-time performance in terms of several engineering application fields. Insufficient ensembled averaging times will lead to too high residual noise in components that are subjected decomposition. The algorithm of CEDANN eliminates part of the noise amplitude within components, effectively solves the issue of too many ensemble averages of the EEMD algorithm, while improving the decomposition efficiency of algorithm. Fig. 13 shows the structure of the proposed decomposition method in CEDANN model.

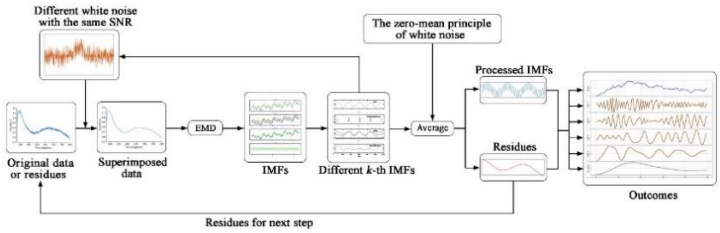

Fig. 13. Structure of proposed decomposition method in CEDANN model.

The algorithm of CEDANN is illustrated below: Suppose $E_n(\bullet)$ represents n-th order component in EMD, $\delta(t)$ represents the noise signal, $x(t)$ is the original signal.

(1) In the original signal $x(t)$, the noise signal $\delta(t)$ is substituted for generating a new signal $s(t)$:

$$s(t) = x(t) + \delta_j(t) \tag{7}$$

where j=1, 2, …, J, it expresses the times of adding noise pairs. For obtaining the first intrinsic mode component imf_1, EMD is performed on the introduced noise signal $s(t)$:

$$s(t) = imf_1 + r_1 \tag{8}$$

The remainder R_1 and the first component $aimf_1$ are yielded by aggregated averaging of the components:

$$aimf_1 = \frac{1}{J}\sum_{j=1}^{J} imf_1^j \tag{9}$$

$$R_1 = s(t) - aimf_1 \tag{10}$$

(2) Subtract $aimf_1$ from the introduced noise signal $s(t)$ for acquiring the residual signal and introducing adaptively decomposed noise component $E_1(\delta(t))$ into residual signals. On that basis, a new signal is obtained, EMD is performed on the signal, the layer decomposition is stopped, and the remainder R_2 and the second component $aimf_2$ are obtained:

$$aimf_2 = \frac{1}{J}\sum_{j=1}^{J} E_1(R_1 + E_1(\delta_j(t))) \tag{11}$$

$$R_2 = s(t) - aimf_1 - aimf_2 \tag{12}$$

(3) Carrying out the above-mentioned second step on the residual signal R_2, several intrinsic mode function (IMF) components and residual term R can be obtained, which can be expressed below

$$aimf_{n+1} = \frac{1}{J}\sum_{j=1}^{J} E_n(R_n + E_n(\delta_j(t))) \tag{13}$$

$$R_n = s(t) - \sum_{i=1}^{n} aimf_i \tag{14}$$

n=1, 2, ..., N, where n represents the number of IMF components.

Several IMF components and the remainder R can express the original signal below:

$$x(t) = \sum_{i=1}^{n} aimf_i + R_n \tag{15}$$

where $x(t)$ represents the original signal, R_n represents the residual signal, $aimf_n$ represents the n-th order IMF component, $s(t)$ represents the noise-introduced signal, and J represents the integration times.

It can be seen from deriving equations (15) that both of them smooth the signal by adding noise to the original signal $x(t)$ to increase the decomposition effect. The sum of the IMF component and the remainder R is approximate to the original signal $x(t)$, and some noises exist in IMF component of each order. The errors of CEDANN decomposition and EEMD are expressed below:

$$e_1 = -\frac{1}{J}\sum_{j=1}^{J}\delta_j(t) \tag{16}$$

$$e_2 = -\frac{1}{J}\sum_{j=1}^{J}E_n(\delta_j(t)) \tag{17}$$

The result achieved through equations (16) and (17) comparison suggests that EEMD error primarily originates from introduced white noise, and multiple integration and averaging lead to the major reduction of the interference with poor partial decomposition effect, and the noise of EEMD. The coefficient setting should not be too large. With the introduction of positive and negative noise pairs, the decomposition is performed for the algorithm of CEDANN, such that component noise is capable of cancelling each other. Second, CEDANN adds the noise components decomposed by EMD, and the small noise amplitude is achieved. EEMD employs complete EMD after adding noise each time, while CEDANN adopts single-layer EMD, such that the running speed of algorithm can be increased.

HRV data fluctuates notably, and considerable factors are found. Thus, HRV is a nonlinear and unstable time series data. Using linear methods or analyze an excessive number of factors is considered to be not appropriate. It increases the workload and the results are not good. This study introduces the novel deep learning framework, termed EBLA, which is self-adaptive fully integrated empirical mode decomposition model to decompose data plus bidirectional long-short memory neural network and optimizes the result weights using the attention mechanism, generally falling into four steps:

(1) Preprocessed data are normalized: Normalize the data, which is convenient for calculation and prevents the data difference from being excessively large, and the model processing is biased toward features with large values.

(2) CEDANN is adopted to decompose into different IMFs: CEDANN effectively addresses the modal aliasing issue that EMD is prone to produce, making the time series feature decomposition more stable and accurate.

(3) The obtained IMFs are input into BiLSTM model for processing: A single processing model fails to effectively extract variable data features in the respective cycle, and splitting the original data in accordance with the type of features and predicting them separately can effectively improve the accuracy.

(4) Attention module is adopted to optimize the obtained weights, and the results overlapping is output: the core of BiLSTM lies in the generation and transmission of hidden states, for example, the feature extraction of data. The attention mechanism can be weighted and strengthened for the increase of the accuracy. Fig. 14 shows the overall structure of the proposed CEDANN model.

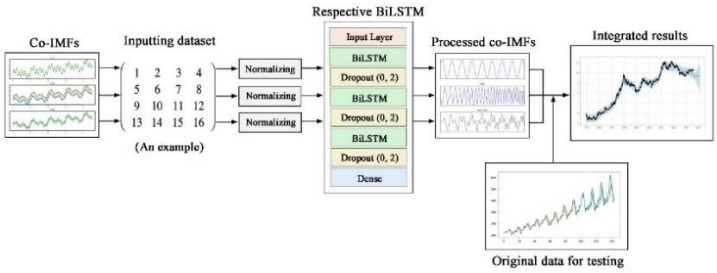

Fig. 14. Structure of the CEDANN model.

Algorithm 1 gives a brief description of the processing of the HRV data and matching with different sleep stages.

Algorithm 1: The proposed CEDANN model.

Input: original signal $RV(t)$, white noise $\omega(t)$, the ensemble number M, data stream $X=\{x_1, x_2, \ldots, x_i\}, x_i \in \mathbf{R}$, epoch I, number of iterations K, error parameters σ, cycle index N, number of decompositions m, white noise data W, sleep-stage labels l.

Function RMF($RV(t)$, $\omega(t)$, M)
  $R_0(t)=RV(t)$;
  j=1;
  while extrema **in** $R_0(t)\geq 2$ **do**
    $\mathrm{IMF}_j(t)$=[];
    for k=1:M **do**
      $\mathrm{IMF}_j(t)=\mathrm{IMF}_j(t)+E_1(R_{j-1}(t)+E_{j-1}(\omega_i(t)))$;
    end for
    $\mathrm{IMF}_j(t)=M^{-1}\mathrm{IMF}_j(t)$;
    $R_j(t)=R_{j-1}(t)-\mathrm{IMF}_j(t)$;
    $j=j+1$;
  end while
  $R(t)=R_j(t)$;
Return $\mathrm{IMF}_j(t)$, $R(t)$, j
Function BiLSTM($\mathrm{IMF}_j(t)$, $R(t)$)
  data= $\mathrm{IMF}_j(t)$ or $R(t)$;
  len= length(data);
  train= data(1: (0.7*len));
  validation= data((0.7*len+1): (0.8*len));
  test= data((0.8*len+1): (0.9*len)), lowest the RMSE, MAE and MAPE during model training;
  $\chi=\Lambda_{\mathrm{data}}$(model, test);
  $G(t)$, $S(t)=\chi$;
Return $G(t)$, $S(t)$
[$G(t)$, $S(t)$, j]= RMF($RV(t)$, $\omega(t)$, M);
for i=1: j **do**
  $G(t)$= BiLSTM($\mathrm{IMF}_i(t)$);
end for
$S(t)$= BiLSTM($R(t)$);
for i=1: j **do**
  $S(t)=G(t)+S(t)$;
end for
$\zeta(t)=S(t)$;
$X \leftarrow x_1, x_2, \ldots, x_i \in \mathbf{R}$;
$O \leftarrow \{\}$;
  for each $i \in N$ **do**
    $H_i^+ \leftarrow x + W_i^+$, $H_i^- \leftarrow x + W_i^-$;
    for $j \in I$ **do**
      $H_{ij}^+ \leftarrow$RMF(H_i^+), $H_{ij}^- \leftarrow$RMF(H_i^-);
    end for
  end for
for $j \in m$ **do**

42: $O \leftarrow \Sigma(\text{BiLSTM}(\text{IMF}_j))$;
43: $\varphi \leftarrow f(O, l)$, $loss \leftarrow |\Im_t(O) - l_t|$;
44: **end for**
Output: $\zeta(t)$, processing result O and matching performance φ.

D. Proposed Semi-supervised Learning Algorithm (GSCM)

In practical applications, most of the data can be represented by graphs, or the actual problems they correspond to are problems based on graph structures, such as social networks, sensor networks, and biological networks. Their essence is graph-based problems, and graph modeling-based methods are more intuitive and interpretable to solve. The semi-supervised algorithms with graph modeling can flexibly process data according to application scenarios and have the advantages of being able to achieve parallelization and having a solid mathematical foundation. Therefore, graph-based semi-supervised learning has received widespread attention and application in recent years. Through knowledge related to graph theory, popular information and inherent geometric structures in data can be mined. In addition, graph theory and popular structures can be well integrated into Euclidean space to improve the performance of model.

In the graph modeling-based semi-supervised learning method, the learning effect of the model depends on the quality of the constructed similarity graph, that is, the quality of the similarity graph directly affects the performance of the semi-supervised learning model. The graph modeling-based semi-supervised learning algorithm first needs to construct a weight graph $G=(V, E)$, $V=(x_1, x_2, \ldots, x_l, x_{l+1}, \ldots, x_n)$, in order to represent a vertex set with labeled samples and unlabeled samples or features as graph vertices, where E represents the edge set, that is to say, the affinity matrix, in which the element S_{ij} describes the similarity between the data points x_i and x_j. Then based on the similarity graph, the label information of the unknown label data sample is calculated. Therefore, semi-supervised learning based on semi-supervision involves the construction of graphs, similarity calculations, setting of loss functions, construction of regular terms, etc.

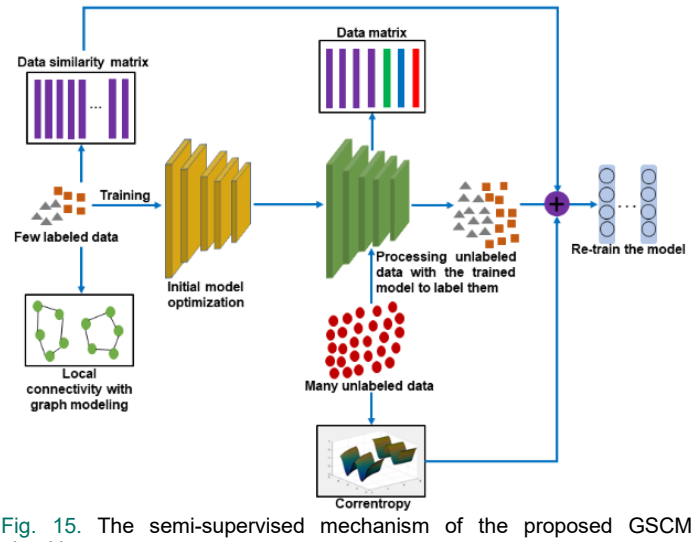

Fig. 15. The semi-supervised mechanism of the proposed GSCM algorithm.

The external knowledge, such as in the diffusion model for time series and spatial-temporal data, have been used in a branch of research. The proposed GSCM algorithm integrated the graph modeling into a deep neural network architecture and achieved a sparse connection between the layers of the proposed framework to prevent over-fitting effectively.

Fig. 15 shows the semi-supervised mechanism in the GSCM algorithm. The GSCM algorithm considers the external knowledge, global and local characteristics of the data. Let the dataset $D=\{x_i|x_i \in \mathbf{R}^m, i=1, 2, \ldots, n\}$, n is the number of samples in D. Among them, $D_l=\{(x_1, y_1), \ldots, (x_l, y_l)\}$ is the labeled sample set, $l<<n$, $D_u=\{x_{l+1}, \ldots, x_n\}$ represents the unlabeled sample set, and Y_l is the label set of previous l labeled samples, the goal of GSCM algorithm is to use D and Y_l to calculate the label set Y_u of the samples in D_u. Let Y_{n*c} represents the initialization label matrix of the samples in D, where c is the number of different labels of the samples in D. Define F_{n*c} as the probability matrix of each class of samples in D, and F_{ij} represents the probability that x_i belongs to the j-th class. Details of the proposed GSCM algorithm are shown in Algorithm 2.

Algorithm 2: The proposed GSCM algorithm.

Input: original graph (G), diagonal matrix (D), α, ξ, labeled data $X_l=\{(x_1, y_1), (x_2, y_2), \ldots, (x_l, y_l)\}$, unlabeled data $X_u=\{x_{l+1}, x_{l+2}, \ldots, x_n\}$, compromise parameter C_l and C_u.
1: Set different N for different datasets for obtaining feature vector sets;
2: **if** $i \neq j$
3: **then** calculate $\boldsymbol{W}$: $w_{ij} = e^{-\frac{\|x_i - x_j\|^2}{2\sigma^2}}$;
4: **else** $w_{ij} = 0$;
5: Calculate $\boldsymbol{S}$: $S = D^{-\frac{1}{2}} W D^{-\frac{1}{2}}$;
6: **for** each iteration **do**
7: Calculate $F^* \leftarrow (1-\alpha)(I-\alpha S)^{-1}Y$;
8: Calculate $F(t+1) \leftarrow \alpha SF(t)+(1-\alpha)Y$, where $\alpha \in [0,1]$, until convergence;
9: $F \leftarrow$ a non-negative matrix of size $n * k$, where n is the number of samples;
10: $n \leftarrow l+u$;
11: $k \leftarrow$ the number of sample categories;
12: $Y \leftarrow$ the sample marker matrix;
13: **if** the marker of the i-th sample is j
14: **then** $y_{ij} = 1$;
15: **else** $y_{ij} = 0$;
16: **for** samples with unknown tags **do**
17: $y_{ij} = 0$;
18: **end for**
19: **end for**
20: Training a model by using X_l;
21: Initialize ω, b and ξ in the model;
22: Initialize $C_u << C_l$;
23: **while** $C_u < C_l$ **do**
24: Calculate (ω, b) and ξ by X_l, X_u, C_l, C_u, y;
25: **while** $\exists \{(i, j)|(y_i y_j<0) \wedge (\xi_i>0) \wedge (\xi_j>0) \wedge (\xi_i+\xi_j>2)\}$ **do**
26: $\omega_i \leftarrow -y_i$;
27: $\omega_j \leftarrow -y_j$;
28: **end while**
29: $C_u \leftarrow \min\{2C_u, C_l\}$;
30: **end while**
Output: $F^*=\lim\{F(t)\}$.

III. Experiments And Results

A. Implementation Details

The optimizer is ADAM, the batch size is 64, the learning rate is set as 0.0005, and the activation function is ReLu. All the experiments are carried out based on a computer equipped with Intel i7-8700 CPU and NVIDIA GeForce GTX1080Ti graphics card. We implement the model based on the PyTorch framework using Python language. We conduct whole experiment based on 10-fold cross-validation mechanism to verify the robust of the proposed framework and avoid the potential overfitting problem. We collected HRV data from 300 subjects, including 150 males and 150 females. Every subject's HRV data has over 3000 data points. Among them, 60% of the dataset is used to train models, 20% of the dataset is applied to test models, and the rest is used for validation. And in statistical analysis of dataset, the p-value by the T-test is generally $p<0.05$ as significant, which means that the probability of the difference between samples caused by sampling error is less than 0.05.

In this study, three evaluation metrics are adopted, which comprise root mean square error (RMSE), mean absolute percentage error (MAPE) and mean absolute error (MAE) [36], [37]. When the three metrics are lower, the model performance is better. Relative to other methods, the proposed model produces better performance. The evaluation metrics are written below

$$MAE = \frac{1}{n}\sum_{i=1}^{n}\left|\hat{y}_i - y_i\right| \tag{18}$$

$$RMSE = \sqrt{\frac{1}{n}\sum_{i=1}^{n}(\hat{y}_i - y_i)^2} \tag{19}$$

$$MAPE = \frac{1}{n}\sum_{i=1}^{n}\left|\frac{\hat{y}_i - y_i}{y_i}\right| \tag{20}$$

Where $\hat{y}_i$ represents the value achieved through processing, and y_i denotes the observed value. In the experiment, support vector regression (SVR) [38], extreme learning machine (ELM) [39], back-propagation neural network (BPNN) [40], ORNN [41], TVF [42] and EIF-NS [43] are set as baseline models.

B. Experimental Results

Optical fiber sensor proves particularly well-suited for ECG signal monitoring, with its distributed measurement capabilities, cost-effectiveness, high sensitivity, and inconspicuous nature, ultimately yielding satisfactory outcomes. But their characteristics such as manufacturing process, size, cost, and feasibility can significantly impact their performance in signal measurement. High-quality sensors offer better signal measurement accuracy. However, complex manufacturing processes can increase the cost. The size of the sensor can also impact its performance. Smaller sensors are more suitable for applications that require high precision and are space-constrained. However, miniaturization can sometimes compromise the sensor's sensitivity and stability. Cost is a crucial factor in the widespread adoption of fiber optic sensors. While they offer superior performance, their high cost can be a barrier for some applications. Lower-cost sensors may not offer the same level of accuracy or durability. Feasibility refers to the ease of integration of the sensor into different systems. Sensors are easy to install and maintain can significantly improve the reliability and efficiency of signal measurement. However, complex installation procedures can increase the overall cost and limit their use in certain applications.

Table I, II, III, IV and Fig. 16 show the experimental results and decomposition results based on different methods respectively.

TABLE I
Experimental results based on SVR and ELM.

	SVR			ELM		
No.	MAE	RMSE	MAPE	MAE	RMSE	MAPE
#1	5.288	5.695	8.253	4.864	5.292	7.577
#2	4.898	5.366	7.646	5.373	5.702	8.395
#3	4.582	4.979	7.168	3.604	4.172	5.600
#4	5.856	6.228	9.162	3.888	4.381	6.060
#5	4.639	5.050	7.262	3.639	4.181	5.671
#6	5.317	5.630	8.326	3.508	4.076	5.466
#7	4.240	4.562	6.630	3.241	3.731	5.045
#8	3.423	4.074	5.344	3.156	3.652	4.922
#9	3.353	3.903	5.243	2.628	3.245	4.090
#10	4.743	5.077	7.454	3.188	3.630	4.989
#11	5.316	5.625	8.361	3.368	3.688	5.278
#12	4.544	4.808	7.127	3.615	3.975	5.663
#13	3.938	4.166	6.174	3.411	3.725	5.342
#14	3.219	3.637	5.037	3.803	4.186	5.964
#15	3.399	3.685	5.332	3.231	3.590	5.071
#16	2.868	3.426	4.505	2.577	3.110	4.041
#17	2.684	3.198	4.227	2.928	3.416	4.606
#18	2.726	3.159	4.282	2.815	3.270	4.418
#19	2.765	3.241	4.342	2.519	2.986	3.947
#20	3.531	3.899	5.552	2.431	2.875	3.808
#21	4.226	4.536	6.645	2.437	3.024	3.817
#22	3.181	3.553	4.986	2.813	3.508	4.398
#23	3.349	3.732	5.252	2.833	3.219	4.345
#24	3.089	3.499	4.837	2.266	2.929	3.523
#25	3.080	3.447	4.819	3.584	3.872	5.626

TABLE II
Experimental results based on BPNN and ORNN.

	BPNN			ORNN		
No.	MAE	RMSE	MAPE	MAE	RMSE	MAPE
#1	3.541	4.316	5.462	4.379	4.923	6.792
#2	2.681	3.816	4.102	4.124	4.738	6.396
#3	2.595	3.736	3.979	4.066	4.627	6.322
#4	2.567	3.705	3.921	3.365	4.059	5.207
#5	2.372	3.551	3.615	3.189	3.859	4.941
#6	2.307	3.373	3.523	2.730	3.409	4.213
#7	2.120	3.127	3.243	2.800	3.312	4.341
#8	2.388	3.123	3.690	2.466	3.012	3.821
#9	2.319	3.009	3.587	3.131	3.538	4.887
#10	2.594	3.167	4.033	3.602	3.958	5.641
#11	3.056	3.461	4.779	4.917	5.181	7.720
#12	3.171	3.557	4.954	3.142	3.494	4.909
#13	3.146	3.475	4.917	4.021	4.266	6.302
#14	2.999	3.385	4.686	3.695	3.992	5.787
#15	4.284	4.523	6.725	3.447	3.748	5.403
#16	3.811	4.122	5.984	2.933	3.305	4.598
#17	4.090	4.422	6.444	2.271	2.743	3.565
#18	2.755	3.178	4.337	3.548	3.905	5.583
#19	3.384	3.713	5.322	3.311	3.670	5.210
#20	1.938	2.440	3.029	3.539	3.860	5.573
#21	3.606	3.903	5.667	3.094	3.427	4.855
#22	2.382	2.856	3.713	2.063	2.563	3.204

#23	2.219	2.771	3.453	2.745	3.130	4.293
#24	3.957	4.202	6.220	2.547	2.984	3.972
#25	3.782	4.015	5.941	2.324	2.784	3.621

TABLE III
Experimental results based on TVF and EIF-NS.

	TVF			EIF-NS		
No.	MAE	RMSE	MAPE	MAE	RMSE	MAPE
#1	1.985	3.007	3.046	11.213	11.402	17.531
#2	1.934	2.789	2.957	7.836	8.088	12.259
#3	1.800	2.557	2.776	7.701	7.930	12.066
#4	1.702	2.507	2.616	9.548	9.726	14.926
#5	1.638	2.423	2.539	8.518	8.703	13.320
#6	1.564	2.195	2.405	9.156	9.306	14.301
#7	1.781	2.335	2.781	9.728	9.867	15.205
#8	1.480	2.023	2.311	10.639	10.749	16.623
#9	1.477	1.995	2.290	14.536	14.601	22.665
#10	1.322	1.919	2.046	4.401	4.565	6.905
#11	1.253	1.757	1.932	5.325	5.432	8.343
#12	1.265	1.778	1.950	4.967	5.100	7.783
#13	1.326	1.687	2.041	3.686	3.820	5.780
#14	1.054	1.481	1.618	4.052	4.207	6.353
#15	1.032	1.419	1.597	4.395	4.499	6.884
#16	1.481	1.733	2.284	4.613	4.702	7.224
#17	1.109	1.660	1.736	7.286	7.352	11.413
#18	1.288	1.648	1.985	5.477	5.557	8.572
#19	0.973	1.251	1.508	6.731	6.787	10.526
#20	0.920	1.189	1.428	5.508	5.563	8.627
#21	0.972	1.385	1.495	4.421	4.512	6.932
#22	1.086	1.448	1.664	3.416	3.548	5.369
#23	1.163	1.580	1.783	13.085	13.142	20.479
#24	1.161	1.548	1.802	4.107	4.228	6.430
#25	1.260	1.664	1.961	11.105	11.164	17.365

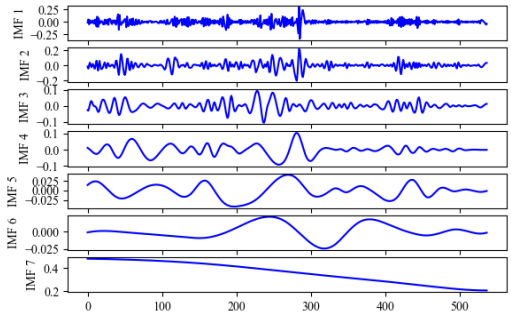

(a)

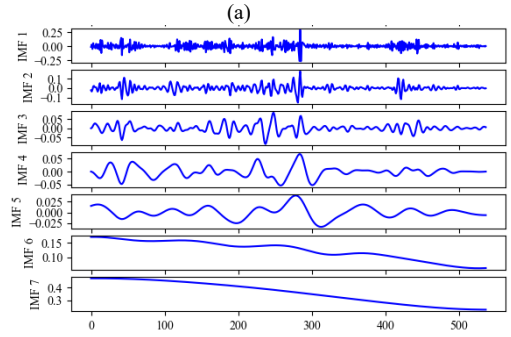

(b)

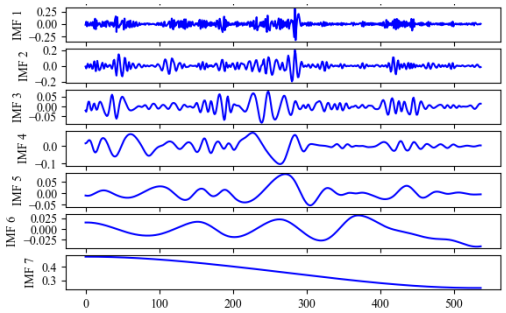

(c)

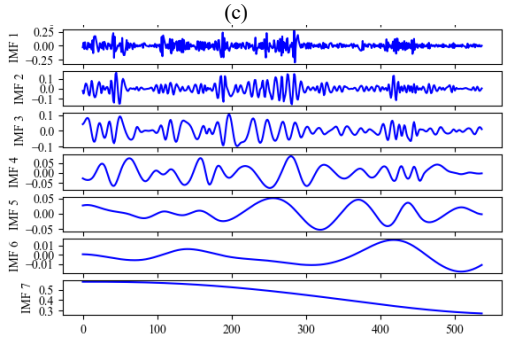

(d)

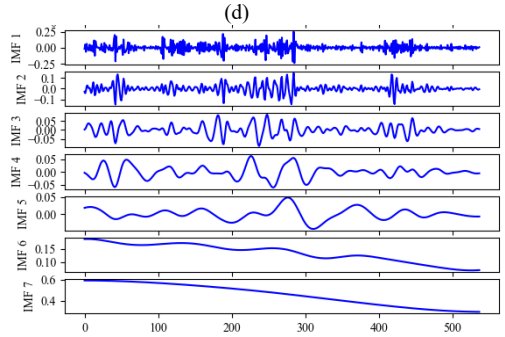

(e)

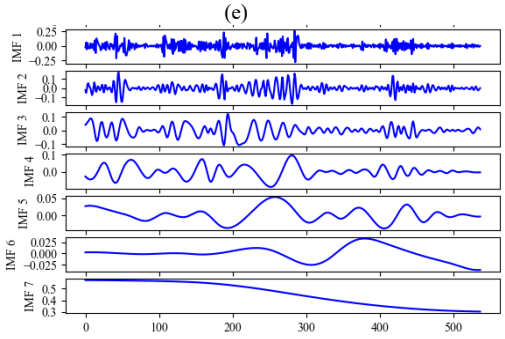

(f)

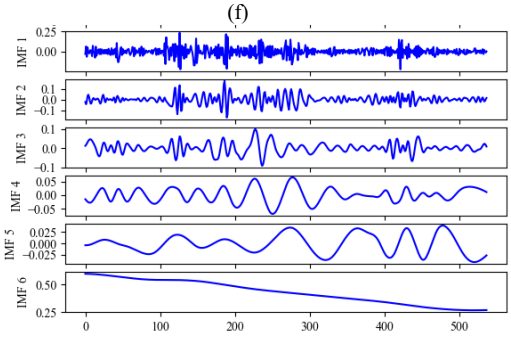

(g)

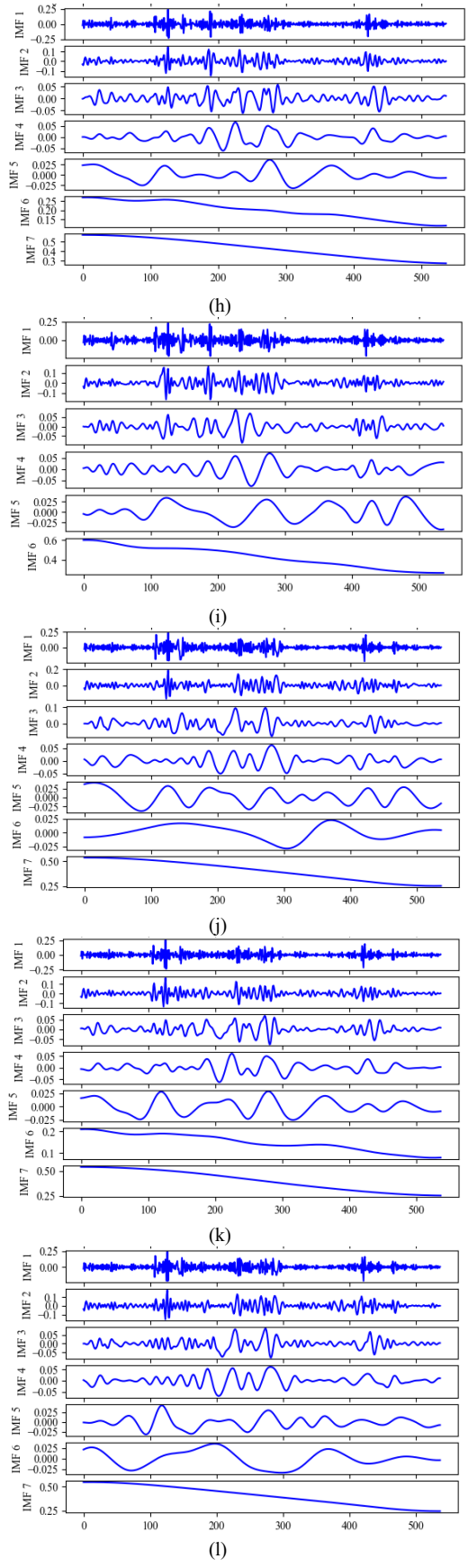

Fig. 16. Decomposition results of four different subjects' HRV data with TVF (a, d, g, i), EIF-NS (b, e, h, k) and CEDANN (c, f, i, l) methods.

TABLE IV
Experimental results based on EBLA framework.

No.	EBLA		
	MAE	RMSE	MAPE
#1	**1.604**	**2.514**	**2.455**
#2	**1.662**	**2.463**	**2.553**
#3	**1.647**	**2.399**	**2.549**
#4	**1.442**	**2.223**	**2.216**
#5	**1.271**	**1.906**	**1.959**
#6	**1.383**	**1.935**	**2.126**
#7	**1.440**	**2.079**	**2.226**
#8	**1.316**	**1.900**	**2.048**
#9	**1.392**	**1.987**	**2.124**
#10	**1.251**	**1.784**	**1.926**
#11	**1.222**	**1.738**	**1.884**
#12	**1.224**	**1.756**	**1.902**
#13	**1.104**	**1.603**	**1.718**
#14	**1.012**	**1.401**	**1.558**
#15	**0.918**	**1.279**	**1.416**
#16	**1.125**	**1.478**	**1.758**
#17	**1.069**	**1.518**	**1.671**
#18	**1.205**	**1.648**	**1.883**
#19	**0.954**	**1.245**	**1.479**
#20	**0.855**	**1.135**	**1.331**
#21	**0.898**	**1.279**	**1.382**
#22	**0.959**	**1.353**	**1.490**
#23	**0.981**	**1.382**	**1.511**
#24	**1.036**	**1.455**	**1.603**
#25	**0.936**	**1.305**	**1.445**

For the extracted HRV data, not all the data are suitable as samples for processing, and preprocessing is required. When sample data are being collected, the size of the sample data should be considered. The excessively small sample data cannot indicate the general law of the HRV data change trend. However, if the data is too large, the training time will be too long. It may even trigger poor convergence. Besides paying attention to the size of the data, when collecting sample data, it is also necessary to consider data loss and data abnormalities arising from equipment failure or other factors. However, the issue data cannot be directly used for HRV data processing, otherwise it will lead to a large deviation in the processing results, such that the issue data should be filled or corrected. Fig. 17 shows the average experimental results with different methods.

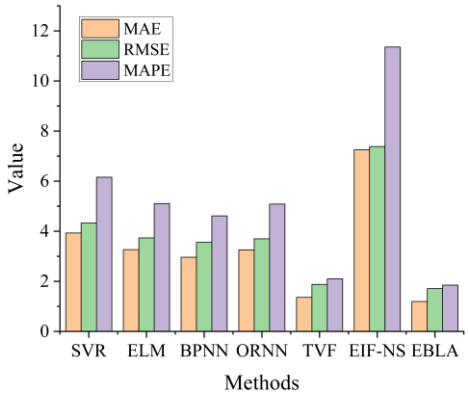

Fig. 17. Average experimental results of different methods.

Due to accidents, such as equipment failure, signal interference, and data transmission failure, the HRV data collected in the process of collecting HRV data fluctuates and deviates from the ground truth [44]. When the sample data is abnormal, it should be corrected in time, otherwise it will affect the training and learning of the model, such that it will not be possible to obtain a more accurate HRV data change law and reduce the processing accuracy. Abnormal data that are common in research, such as extreme values and glitches. To be specific, the extreme value is divided into maximal value and minimal value, the maximal value means that the sample value at the non-peak time exceeds the sample value at the peak time; and the minimal value means that the sample value at the non-trough time is smaller than the current value. Furthermore, a glitch suggests that the sample value at a certain time point is notably larger or much smaller than the sample value at its adjacent time point. In general, the data is processed in accordance with the characteristics of abnormal data [45].

The HRV value in a short time range slightly varies, and little difference is identified in the HRV value at adjacent moments. If the absolute value of adjacent HRV values exceeds the allowable error threshold, the HRV value at this point turns out to be abnormal. The equation for judging abnormal data is expressed:

$$max[\,|D_{t+1}-D_t|,|D_t-D_{t-1}|] > \varepsilon(t) \tag{21}$$

where D_t denotes the abnormal HRV value at t, $\varepsilon(t)$ represents the error threshold, $D_{t\text{-}1}$ expresses the HRV value at t-1, and D_{t+1} denotes the HRV value at t+1.

When the abnormal data is detected, the value should be corrected and divided into the following four steps:

(1) The HRV values at two moments before and after the time corresponding to the abnormal HRV value are selected, with the aim of ensuring a slight change before and after the adjacent values of HRV values, such that the equation of the average HRV value at five adjacent moments of D_t is written as

$$E_1 = \frac{A_{t+2}+A_{t+1}+A_t+A_{t-1}+A_{t-2}}{5} \tag{22}$$

where E_1 is the mean value of HRV.

(2) Determine the HRV mean value of the three adjacent moments of D_t, the equation is defined as

$$E_2 = \frac{A_{t+1}+A_t+A_{t-1}}{3} \tag{23}$$

where E_2 is the mean value of HRV.

(3) Determine the HRV mean value of two adjacent moments of D_t, the equation is expressed as

$$E_3 = \frac{A_{t+1}+A_{t-1}}{2} \tag{24}$$

where E_3 is the mean value of HRV.

(4) Determine the corrected HRV value, the equation is presented as

$$G_t = w_1E_1 + w_2E_2 + w_3E_3 \tag{25}$$

where w_1, w_2 and w_3 are corrected weights, and G_t is the corrected HRV value.

Moreover, since sample data are insufficient under the effect of some other factors, the HRV numerical processing can be conducted to fill in the missing data periodically because of its timeliness, with the aim of increasing the processing accuracy. Although the time is different, the HRV values at the identical time are similar. The HRV data at the previous adjacent time point where the missing data is located is averaged as the data that should be filled. Likewise, the HRV values at the adjacent and preceding moments at different time points are similar, such that the average value of the HRV data at the adjacent previous time point at the time point where the missing data is located can be taken as the data that should be filled.

The goal of data normalization is to scale the sample data to a fixed range. After normalization, the sample data are capable of avoiding the large deviation due to different dimensions and attributes. Moreover, the algorithm iteration convergence speed can be increased, thus expediting the improvement of HRV processing accuracy. The min-max method is adopted for normalization, which uses the maximal value for calculation processing, and fixes the sample data between the [0, 1] range through a linear map. The min-max normalization is defined as

$$P = \frac{A-A_{min}}{A_{max}-A_{min}} \tag{26}$$

where A_{max} denotes the maximal value in the sample, P represents the value after normalization, A refers to the original value, and A_{min} is the minimal value in the sample.

After obtaining the predicted results, it is necessary to use the denormalization method should be employed for recovering the results. The denormalization is defined as follows

$$Q = P \times (A_{max} - A_{min}) + A_{min} \tag{27}$$

We also used signal processing techniques such as wavelet analysis to decompose the signal into multiple frequency bands, identify and remove the data of the interference frequency bands. This method is particularly effective for processing high-frequency noise and mixed signals. Meanwhile, by analyzing the time domain and frequency domain characteristics of the vibration signal, multiple thresholds are set to distinguish different types of interference signals. This can effectively identify and filter out environmental interference and human interference, thereby reducing the false alarm rate.

HRV data has characteristics such as uncertainty, timeliness, nonlinearity, etc., and other external factors make HRV data more unstable. Accordingly, the CEDANN algorithm is used to compress the frequency aliasing area and enhance the convergence, which exhibits a strong resolution ability for nonlinear and uncertain signals with different frequency components. Moreover, the respective subsequence of HRV data acquired after decomposition using the CEDANN algorithm exhibits regularity, which can help improve the accuracy. Fig. 18 illustrates the processing results of ECG signal.

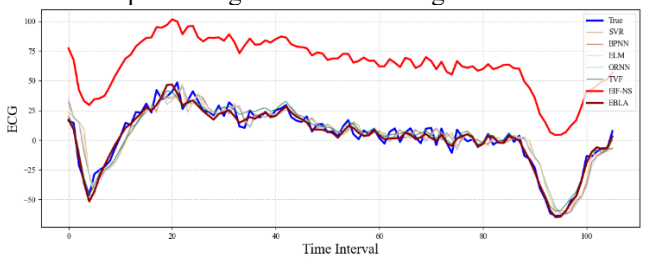

(a) #13

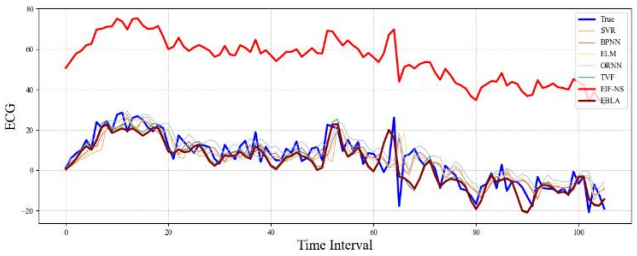

(b) #14

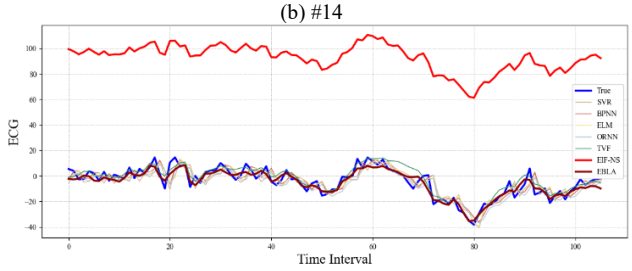

(c) #19

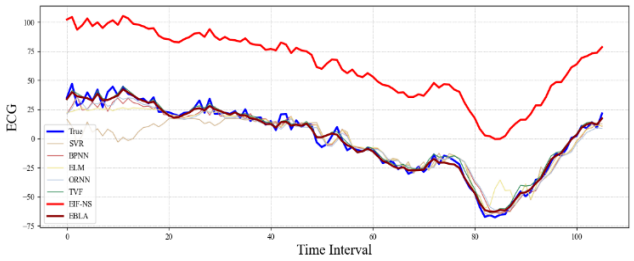

(d) #21

Fig. 18. The ECG processing results of four subjects by different methods.

After CEDANN decomposition, the number of IMF components is 11 and the number of residual components is 1. The same operation will be performed on the above-described components below. First, the IMF component and residual component obtained by decomposing are unified into three hours of data volume, and the change of HRV data is predicted. In accordance with the time factor of HRV data processing, the data change trend in historical HRV data is divided into 12 groups in total. Before 11 sets of HRV data are set as training sets to train the model. Afterward, the preprocessed IMF and residual components are substituted into the BiLSTM model for signal processing, and 12 sets of processing results are obtained. Furthermore, all the processing results are accumulated, with the aim of obtaining the final HRV data processing result and the matching relationship between HRV and sleep stages.

By analyzing the results achieved through experiments, some conclusions can be drawn by us:

(1) The proposed conventional machine learning model is superior to the deep learning method, such that the neural networks are proven with advantages in the processing of the nonlinear HRV data during sleep;

(2) The EBLA model outperforms other methods, displaying more notable advantages in HRV monitoring corresponding with the sleep stages. The reason is that the model can aggregate the node's neighbor node feature. Thus, spatial features of all HRV data will be obtained more effectively;

(3) The finer the classification of sleep stages, the higher the degree of matching between HRV and sleep stages;

(4) Different from other models, the proposed EBLA model can be applied to HRV processing and adopted to tackle other vital signs signal processing tasks with spatial-temporal modeling.

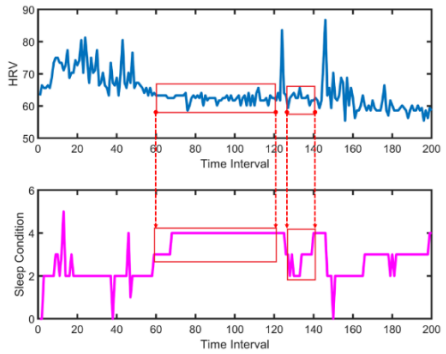

(a) #13

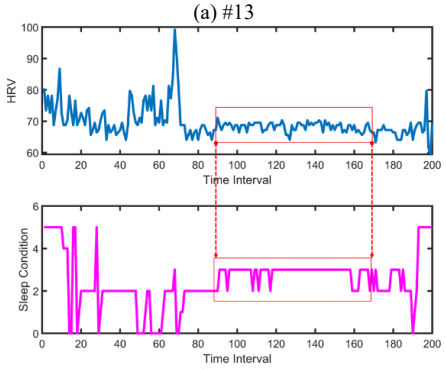

(b) #14

Fig. 19. The results of matching between HRV and sleep conditions (0: WAKE; 1: S1; 2: S2; 3: S3; 4: S4; 5: REM).

Fig. 19 shows the matching results of the HRV and different sleep stages. The sleep stage can be divided into five stages: wake stage (W), stage 1 (S1), stage 2 (S2), stage 3 (S3), stage 4 (S4) and REM stage (REM) [46]. In general, better sleep can not only help people eliminate fatigue and restore the normal functioning of various systems in the human body, but also help people relieve stress and promote body growth and development. This indicates that sleep is crucial for the human body. However, with the acceleration of the pace of life in modern society and the increase of life pressure, Sleep-disorder has become the main health problem people face during sleep. At present, the sleep examination used for patients in hospitals mainly involves multi-channel sleep monitoring. The electrode is directly in contact with the human skin, and the operation is complex. Although it can ensure a certain degree of monitoring accuracy, it consumes a lot of manpower and material resources, and has a certain impact on the sleep of the subjects, which can also have a certain impact on the accuracy of monitoring data. The traditional sleep staging method based on a single ECG signal can no longer meet human requirements for accurate recognition of different sleep stages. Therefore, this paper proposes a deep learning model based on R-R interval sequence, HRV and sleep stages matching, which can effectively extract the temporal and spatial features of HRV

signals. It also provides a new approach for non-invasive monitoring of sleep conditions.

Feature extraction and representation is an important part of ECG signal processing. Energy entropy, power spectrum entropy, singular spectrum entropy and fuzzy entropy are used to extract the entropy value features of the main IMF components to construct the initial feature vector. However, the initial feature dimension obtained is high and may contain redundant features, therefore, we used t-SNE to visualize the original representation and the representation learned through GSCM [47], which is shown in Fig. 20. The data points in the three-dimensional graphs of the principal component analysis (PCA) and locality preserving projection (LPP) dimensionality reduction methods are relatively close, there is cross-aliasing phenomenon, and there are some discrete points, while the GSCM algorithm can intuitively distinguish the categories. Therefore, the comparison of analysis results demonstrates the superiority of the proposed GSCM algorithm.

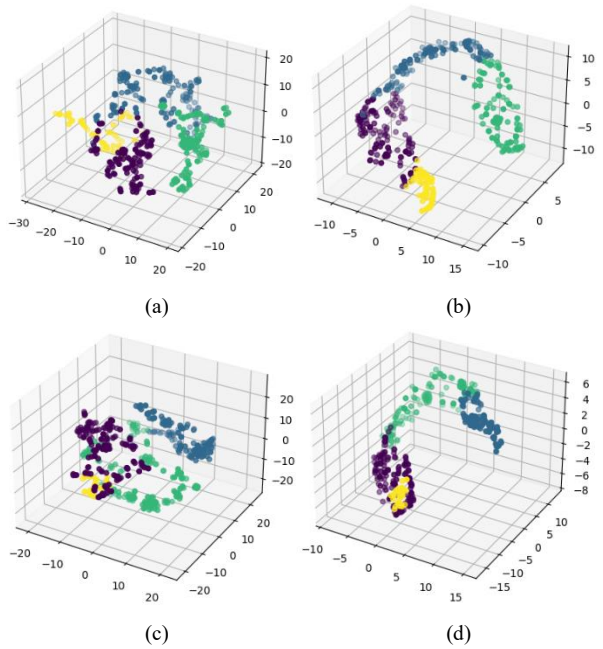

Fig. 20. The t-SNE plots on data processing. (a), (c): The original sample representations; (b), (d): The computed sample representations of GSCM.

C. Parameter Analysis

Fine-tuning parameters in a semi-supervised learning model is of paramount importance for achieving optimal performance. Semi-supervised learning is a machine learning paradigm that uses both labeled and unlabeled data for training. The labeled data is often scarce and expensive to obtain, while the unlabeled data is abundant and inexpensive. The goal is to make the best use of both types of data to improve the learning performance.

The performance of a semi-supervised learning model heavily depends on the fine-tuning of its parameters. These parameters control various aspects of the model, such as the balance between the labeled and unlabeled data, the complexity of the model, etc. If these parameters are not properly tuned, the model may overfit or underfit the data, leading to poor generalization performance on unseen data.

Fine-tuning parameters is also crucial for leveraging the unlabeled data effectively. In semi-supervised learning, the unlabeled data provides additional, indirect information about the underlying data distribution. However, how to use this information effectively is controlled by the parameters of the model. If these parameters are not well-tuned, the model may fail to exploit the unlabeled data, or even worse, it may be misled by the unlabeled data. Overall, fine-tuning parameters in a semi-supervised learning model is a critical step that can significantly affect the model's performance. In experiments, we tuned the γ_1 and γ_2 are both within the range of {0.5, 1.0, 1.5, 2.0, 2.5}, respectively. Fig. 21 shows the impact of changes in γ_2 on model performance when γ_1 remains unchanged. Fig. 22 displays the impact of changes in γ_1 and γ_2 on the experimental results, respectively.

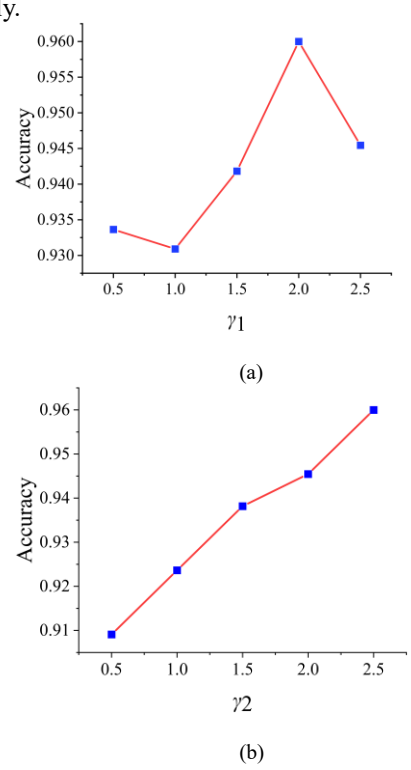

Fig. 21. Experimental results with different (a) γ_1 and (b) γ_2 values.

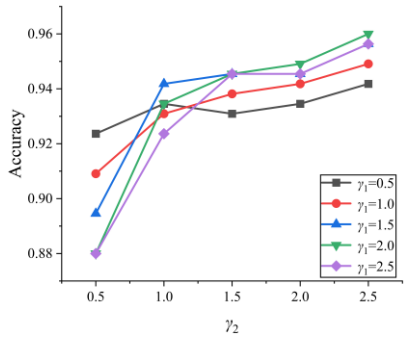

Fig. 22. Impact of changes in γ_1 and γ_2 on the experimental results.

D. Ablation Study

The ablation study can be used to understand the contribution of different components of a model to its overall performance. It involves systematically removing or modifying parts of the model, such as layers, connections, or specific modules, and observing the impact on the model's performance. The importance of ablation studies in deep learning models lies in their ability to provide insights into the inner workings of complex models.

By conducting an ablation study, which parts of the model are crucial for its performance and which parts are less important can be identified. This can guide the development of more efficient models, as unnecessary components can be removed without significantly affecting performance.

Furthermore, ablation studies can help in understanding how different components of a model interact with each other. This can lead to the discovery of novel, more effective architectures or training strategies.

In experiments, to confirm the importance of mode decomposition and semi-supervised learning mechanism in the proposed model, we replaced the mode decomposition module (EBLA-ND), semi-supervised learning algorithm (EBLA-NS), and replaced both mode decomposition module and semi-supervised learning algorithm (EBLA-NSD). By comparing the MAE, RMSE and MAPE, EBLA exhibits the best performance compared to another two variant models. Table V and Fig. 23 show the experimental results, respectively. Experimental results effectively prove the importance and necessity of the mode decomposition and semi-supervised learning mechanism.

TABLE V
Experimental results based on different variant models

	EBLA-NSD		EBLA-NS		EBLA-ND		EBLA	
No.	MAE	RMSE	MAE	RMSE	MAE	RMSE	MAE	RMSE
#1	6.095	7.799	5.406	7.181	3.666	4.678	**3.661**	**4.673**
#2	5.464	7.147	5.652	7.452	4.172	5.496	**3.931**	**5.055**
#3	6.196	7.735	5.431	7.001	3.432	4.293	**3.140**	**3.921**
#4	7.434	9.404	6.179	7.946	3.813	5.196	**3.788**	**4.906**
#5	5.193	6.796	5.415	7.035	5.033	5.998	**3.489**	**4.223**
#6	6.783	8.079	6.899	8.993	3.291	3.980	**2.927**	**3.644**
#7	7.531	9.169	6.266	7.970	4.604	5.775	**4.013**	**5.406**
#8	5.329	7.143	4.742	6.496	3.302	4.127	**3.180**	**4.034**
#9	7.350	9.462	4.913	6.630	4.636	5.761	**4.401**	**5.693**
#10	5.843	7.683	5.837	7.640	4.651	5.836	**4.547**	**5.803**

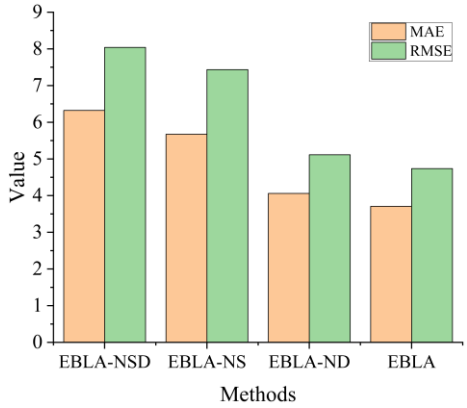

Fig. 23. Average experimental results of different variant models.

IV. Discussion

A novel optical fiber sensor proposed by us based on fiber interferometer that can be used to monitor human physiological parameters like HRV, which can be used to generate an ECG effectively. The ECG data can then be used to calculate HRV, a measure of the human response to stress and disease. Deep learning, a branch of machine learning and artificial intelligence, can be applied to analyze these complex datasets. By training on large amounts of ECG and HRV data, deep learning algorithms can learn to identify patterns and make predictions, such as detecting heart disease or predicting a heart attack. Thus, the combination of these technologies can lead to more accurate, timely, and personalized healthcare.

Meanwhile, in this study, the proposed CEDANN model is a data-driven decomposition technique commonly used in signal processing and time series analysis. When combined with semi-supervised learning, it can offer several advantages compared to other models for various applications. CEDANN decomposes complex time series data into a set of IMFs and a residual component. This decomposition helps in capturing the underlying modes and patterns in the data, making it suitable for feature extraction. CEDANN is adaptive, meaning it can adjust its decomposition based on the input data. This adaptivity can help it capture non-stationary and non-linear patterns, which can be challenging for other models. CEDANN separates the data into IMFs and a noise component, which can be advantageous in cases where the signal of interest is mixed with noise. By isolating the noise component, it becomes easier to denoise the data, leading to better feature extraction and model performance.

Semi-supervised learning is a machine learning mechanism that leverages both labeled and unlabeled data for training. When combined with CEDANN, it can help improve the model's performance by using the decomposed features from CEDANN as inputs for the learning algorithm. This can be particularly useful when labeled data is limited, as the model can exploit the structure in the data revealed by CEDANN. The effectiveness of CEDANN combined with semi-supervised learning can vary depending on the specific application and dataset. The choice of model and approach should be guided by the characteristics of the data and the objectives of the analysis. However, when applied appropriately, CEDANN with semi-supervised learning can offer significant advantages in terms of feature extraction, adaptability, and robustness, making it a valuable tool for time series analysis and related tasks.

The proposed GSCM algorithm is a graph modeling-based semi-supervised learning method used for classification and label propagation tasks. GSCM allows for flexibility in how the graph is constructed. Depending on the application, we can define the similarity or affinity measure between data points to create the graph. This adaptability makes it suitable for various types of data, such as text, images, and sensor data. In regions of the data space with sparse data points, GSCM can effectively propagate labels from more densely populated regions, aiding in the classification of data in areas with limited information. GSCM is conceptually simple and easy to understand, which can be advantageous when

explaining and justifying the algorithm's results to stakeholders or in educational settings. GSCM has shown competitive or state-of-the-art performance in various classification and label propagation tasks, especially when the data's underlying structure can be well represented by the graph.

In practical, there are some potential limitations within the proposed framework. First, the modal decomposition method may have modal aliasing problems, resulting in the decomposed signal not accurately reflecting the characteristics of the original signal, which in turn affects the accuracy of subsequent analysis. For ECG and HRV data, feature extraction may be inaccurate, affecting the analysis of sleep stages. Secondly, semi-supervised learning relies on a small amount of labeled data and a large amount of unlabeled data. If the labeled data is of low quality or insufficiently representative, it will affect the training effect of the model. In the future, to overcome these defects, more effective modal decomposition algorithms can be designed to reduce modal aliasing, such as improve the parameter settings of existing algorithms or develop new adaptive algorithms. As for data, the quality and representativeness of labeled data should be improved, which can be achieved through a more rigorous screening and labeling process. Meanwhile, we will develop more advanced self-supervised learning methods combined with semi-supervision for utilizing the potential information of unlabeled data. In addition, customized methods for the characteristics of ECG and HRV data can be further explored to improve the applicability and effectiveness of the combined method in this field.

V. Conclusion

In this paper, we propose a novel optical fiber sensor based on fiber interferometer that can be used to monitor human vital signs signal, such as ECG, BCG and HRV effectively and accurately. Moreover, in order to address the failure of optical fiber sensor based on banding loss, such as improper transmission and storage, data missing and data anomaly in human ECG signal monitoring, a novel deep learning framework (EBLA), is proposed for extracting spatial and temporal features for the human vital signs signal for detecting and measuring the ECG signal better with the proposed optical fiber sensor. Moreover, the HRV can be extracted from the raw ECG signal during human sleep. The proposed CEDANN module can overcome the uncertainty and nonlinearity in the long-term HRV data processing characteristics. The CEDANN module decomposes the historical HRV sequence into several IMF components and residual components. The function of associating the historical data with the future data is used through the dynamic feedback characteristics and memory of the BiLSTM model, with the aim of processing the IMFs and residual components of multiple different frequencies. Meanwhile, the proposed semi-supervised algorithm (GSCM) can reveal the data relationship and obtain the global sample structure from the raw ECG signal with external knowledge better. In general, the proposed EBLA model improves the precision, resilience, and adaptability of vital signs monitoring systems, rendering it an invaluable instrument in the domains of healthcare monitoring and related biomedical applications. In the future, devices can be upgraded to increase the number of network layers, the number of neurons, the time step, and so forth. And another raw signals, such as BCG and polysomnography (PSG) signal, can be collected and analyzed from more subjects of different body types and ages, in order to improve the versatility of the proposed optical fiber sensor and verify the robustness of the proposed model.

Acknowledgements

The authors gratefully acknowledge the financial supports of Non-wearable and non-invasive photonic sleep monitoring system based on optical fiber sensor with machine learning (HKPU 1-WZ01) and Non-wearable and non-invasive photonic smart health monitoring system for atrial fibrillation diagnosis based on optical fiber sensor with machine learning (HKPU 1-CD8N).

References

[1] Liu, Zheng, *et al*. "Analytical optimization of wideband nonlinear optical fiber communication systems." *Optics Express* 30.7 (2022): 11345-11359.
[2] Li, Chao, *et al*. "Optical fiber nonlinearity equalizer with support vector regression based on perturbation theory." *Optics Communications* 507 (2022): 127627.
[3] Li, Mingyu, and Shaowei Wang. "End-to-end learning for chromatic dispersion compensation in optical fiber communication." *IEEE Communications Letters* 26.8 (2022): 1829-1832.
[4] Yin, Zixiao, *et al*. "Pathological pallidal beta activity in Parkinson's disease is sustained during sleep and associated with sleep disturbance." *Nature Communications* 14.1 (2023): 5434.
[5] Gallego-Martínez, Juan José, *et al*. "Devices for monitoring oenological processes: A review." *Measurement* (2024): 114922.
[6] Wen, Xin, *et al*. "A feasible feature extraction method for atrial fibrillation detection from BCG." *IEEE Journal of Biomedical and Health Informatics* 24.4 (2019): 1093-1103.
[7] Pathak, Nidhi, Anandarup Mukherjee, and Sudip Misra. "SemBox: Semantic Interoperability in a Box for Wearable e-Health Devices." *IEEE Journal of Biomedical and Health Informatics* (2022).
[8] Wang, Yuying, *et al*. "Development of fabrication technique and sensing performance of optical fiber humidity sensors in the most recent decade." *Measurement* (2023): 112888.
[9] Hou, Liangtao, *et al*. "Ultra-sensitive optical fiber humidity sensor via Au-film-assisted polyvinyl alcohol micro-cavity and Vernier effect." *IEEE Transactions on Instrumentation and Measurement* 71 (2022): 1-9.
[10] Wang, Qing, *et al*. "Assessment of heart rate and respiratory rate for perioperative infants based on ELC model." *IEEE Sensors Journal* 21.12 (2021): 13685-13694.
[11] Chen, Weijuan, *et al*. "Non-invasive measurement of vital signs based on seven-core fiber interferometer." *IEEE Sensors Journal* 21.9 (2021): 10703-10710.
[12] Wang, Qing, *et al*. "Non-Invasive Human Ballistocardiography Assessment Based on Deep Learning." *IEEE Sensors Journal* (2023).
[13] Lyu, Weimin, *et al*. "Non-invasive measurement for cardiac variations using a fiber optic sensor." *IEEE Photonics Technology Letters* 33.18 (2021): 990-993.
[14] Chen, Shuyang, *et al*. "Ballistocardiography monitoring system based on optical fiber interferometer aided with heartbeat segmentation algorithm." *Biomedical Optics Express* 11.10 (2020): 5458-5469.
[15] Shi, Chaoyang, *et al*. "Development of an FBG-Based Wearable Sensor for Simultaneous Respiration and Heartbeat Measurement." *IEEE Transactions on Instrumentation and Measurement* 72 (2022): 1-9.

[16] Wang, Ying, *et al*. "Noninvasive measurement of the vital signs of cancer patients with a dual-path microbend fiber sensor." *Biomedical Optics Express* 13.2 (2022): 982-994.
[17] Zhang, Yi, Zhihao Chen, and Hwan Ing Hee. "Noninvasive measurement of heart rate and respiratory rate for perioperative infants." *Journal of Lightwave Technology* 37.11 (2019): 2807-2814.
[18] Jarczok, Marc N., *et al*. "Heart rate variability in the prediction of mortality: A systematic review and meta-analysis of healthy and patient populations." *Neuroscience & Biobehavioral Reviews* 143 (2022): 104907.
[19] Faust, Oliver, *et al*. "Heart rate variability for medical decision support systems: A review." *Computers in Biology and Medicine* (2022): 105407.
[20] Zhang, Weijie, *et al*. "CTCNet: A CNN Transformer capsule network for sleep stage classification." *Measurement* 226 (2024): 114157.
[21] Zhao, Tao, *et al*. "Non-contact Monitoring of Heart Rate Variability Using A Fiber Optic Sensor." *IEEE Internet of Things Journal* (2023).
[22] Ge, Zhao, *et al*. "Enabling variable high spatial resolution retrieval from a long pulse BOTDA sensor." *IEEE Internet of Things Journal* (2022).
[23] Galli, Alessandra, Giada Giorgi, and Claudio Narduzzi. "Accurate ECG monitoring by Gaussian feature streaming." *Measurement* 223 (2023): 113757.
[24] Gouveia, Carolina, *et al*. "Bio-Radar Cardiac Signal Model Used for HRV Assessment and Evaluation Using Adaptive Filtering." *IEEE Transactions on Instrumentation and Measurement* 71 (2022): 1-10.
[25] Pant, Himanshu, Hitesh Kumar Dhanda, and Sachin Taran. "Sleep apnea detection using electrocardiogram signal input to fawt and optimize ensemble classifier." *Measurement* 189 (2022): 110485.
[26] Kumar, Mohit, *et al*. "ANAF-IoMT: A novel architectural framework for IoMT-enabled smart healthcare system by enhancing security based on RECC-VC." *IEEE Transactions on Industrial Informatics* 18.12 (2022): 8936-8943.
[27] Shahbakhti, Mohammad, *et al*. "Discrimination of Wakefulness from Sleep Stage I Using Nonlinear Features of a Single Frontal EEG Channel." *IEEE Sensors Journal* 22.7 (2022): 6975-6984.
[28] Shao, Shiliang, *et al*. "Obstructive sleep apnea detection scheme based on manually generated features and parallel heterogeneous deep learning model under IoMT." *IEEE Journal of Biomedical and Health Informatics* 26.12 (2022): 5841-5850.
[29] Weng, Peiyu, *et al*. "Fuzzy Approximate Entropy of Extrema Based on Multiple Moving Averages as a Novel Approach in Obstructive Sleep Apnea Screening." *IEEE Journal of Translational Engineering in Health and Medicine* 10 (2022): 1-11.
[30] Xue, Wei, *et al*. "Accurate multi-target vital signs detection method for FMCW radar." *Measurement* 223 (2023): 113715.
[31] Reyes-González, Luis, Luis Rodríguez-Cobo, and José-Miguel López-Higuera. "Comparison of Ballistocardiogram Processing Methods Based on Fiber Specklegram Sensors." *IEEE Sensors Journal* 22.21 (2022): 20524-20530.
[32] Gharghan, Sadik Kamel, and Huda Ali Hashim. "A comprehensive review of elderly fall detection using wireless communication and artificial intelligence techniques." *Measurement* (2024): 114186.
[33] Arpaia, Pasquale, *et al*. "Conceptual design of a machine learning-based wearable soft sensor for non-invasive cardiovascular risk assessment." *Measurement* 169 (2021): 108551.
[34] Huang, Norden E., *et al*. "The empirical mode decomposition and the Hilbert spectrum for nonlinear and non-stationary time series analysis." *Proceedings of the Royal Society of London. Series A: mathematical, physical and engineering sciences* 454.1971 (1998): 903-995.
[35] Wu, Zhaohua, and Norden E. Huang. "Ensemble empirical mode decomposition: a noise-assisted data analysis method." *Advances in Adaptive Data Analysis* 1.01 (2009): 1-41.
[36] Wang, Qing, *et al*. "A Spatial-Temporal Graph Model for Pronunciation Feature Prediction of Chinese Poetry." *IEEE Transactions on Neural Networks and Learning Systems* (2022).
[37] Du, Changde, *et al*. "Structured neural decoding with multitask transfer learning of deep neural network representations." *IEEE Transactions on Neural Networks and Learning Systems* 33.2 (2020): 600-614.
[38] Huang, Huajuan, Xiuxi Wei, and Yongquan Zhou. "An overview on twin support vector regression." *Neurocomputing* 490 (2022): 80-92.
[39] Gaspar, Angel, *et al*. "An optimized Kernel Extreme Learning Machine for the classification of the autism spectrum disorder by using gaze tracking images." *Applied Soft Computing* 120 (2022): 108654.
[40] Hosseini, Shahab, Rashed Poormirzaee, and Mohsen Hajihassani. "Application of reliability-based back-propagation causality-weighted neural networks to estimate air-overpressure due to mine blasting." *Engineering Applications of Artificial Intelligence* 115 (2022): 105281.
[41] Asha, A., *et al*. "Optimized RNN-based performance prediction of IoT and WSN-oriented smart city application using improved honey badger algorithm." *Measurement* 210 (2023): 112505.
[42] Jamei, Mehdi, *et al*. "Monthly sodium adsorption ratio forecasting in rivers using a dual interpretable glass-box complementary intelligent system: Hybridization of ensemble TVF-EMD-VMD, Boruta-SHAP, and eXplainable GPR." *Expert Systems with Applications* 237 (2024): 121512.
[43] Caldeira, A., and R. Coelho. "EEMD-IF Based Method for Underwater Noisy Acoustic Signals Enhancement in Time-Domain." *IEEE Signal Processing Letters* 30 (2023): 294-298.
[44] Lee, Song-Hong, *et al*. "Reconstruction Attacks in Template-Based ECG Biometric Recognition Systems." *IEEE Internet of Things Journal* (2023).
[45] Han, Honggui, *et al*. "Self-Supervised Deep Clustering Method for Detecting Abnormal Data of Wastewater Treatment Process." *IEEE Transactions on Industrial Informatics* (2023).
[46] Levy, Jeremy, *et al*. "Deep learning for obstructive sleep apnea diagnosis based on single channel oximetry." *Nature Communications* 14.1 (2023): 48.
[47] Van der Maaten, Laurens, and Geoffrey Hinton. "Visualizing data using t-SNE." *Journal of Machine Learning Research* 9.11 (2008).